Soft Matter

PAPER

View Article Online
View Journal | View Issue

Cite this: *Soft Matter*, 2026, **22**, 1994

The effect of thioester linkages on the stability of the ferroelectric nematic phase

Gytis Stepanafas, [a] Stevie Brown, [a] Ewan Cruickshank, †[a] Grant J. Strachan, [ab] John M. D. Storey, [a] Corrie Imrie ‡[a] and Rebecca Walker *[a]

Received 5th December 2025,
Accepted 31st January 2026

DOI: 10.1039/d5sm01206f

rsc.li/soft-matter-journal

The synthesis and characterisation of thirteen sulfur-based liquid crystals are reported, based on the molecular backbone of RM734 and containing thioester linkages. Ten of these materials are new examples of ferroelectric nematogens. Phase transition temperatures are compared for systematic changes to molecular structure including the position and extent of fluorination, and the nature of lateral and terminal substituents. The new materials are compared with their ester-linked counterparts. In line with expected behaviour of the nematic phase, replacement of an ester with a thioester raised T_{NI}, but N_F phase stability upon making this change proved more variable. These findings remain in line with the general view that the formation of the N_F phase is not solely governed by the magnitude of the molecular dipole moment, but is able to be tuned by the interplay of steric and electronic effects endowed by different molecular fragments.

Introduction

The recent groundbreaking discovery of proper ferroelectricity in low molar mass liquid crystals[1] heralded a new era of both fundamental and experimental research in the field, aiming to understand and exploit the fantastic properties of the ferroelectric nematic phase, N_F, for electrooptical applications. A polar variant of the conventional nematic phase, N, the N_F phase has huge application potential, exhibiting switchable electric polarisation and non-linear response comparable in magnitude to that of solid crystalline ferroelectrics while retaining the fluidity and self-healing ability vital in electrooptical devices.[2–10] The vast majority of compounds exhibiting the phase can be categorised by a limited number of molecular templates. The molecular archetypes for the N_F phase are the two 'flagship' materials of groups in Europe and Asia, RM734[11,12] and DIO,[13] respectively and UUQU-4N,[14] for which a room-temperature stable N_F phase was discovered, Fig. 1. Liquid crystal chemists sought to establish design rules for the N_F phase through the creation of large libraries of molecules with structures based on these three templates.[15–18] While some fundamental features quickly became apparent: the necessity for a large longitudinal molecular dipole moment to encourage ferroelectric ordering of molecules, and some degree of lateral bulk, robust structure–property relationships have yet to be established. Nonetheless, the surge in new materials has led to the discovery of numerous other new proper ferroelectric phases in the 'ferroelectric nematic realm', including polar variants of the chiral nematic, N_F*,[19–22] SmA and SmC phases (SmA_F and SmC_F),[23–32] the antiferroelectric N_X[33–37] and SmA_{AF} phases,[38,39] and heliconical ferroelectric nematic (N_{TBF})[40–42] and smectic (SmC^H_P) phases.[38,43]

Sulfur-containing liquid crystal materials are attractive candidates for use in liquid crystal display technologies,[44] liquid crystal lenses,[45] and liquid crystal lasers,[46] owing to their enhanced values of optical birefringence[47,48] compared with structurally analogous molecules instead containing oxygen-based functionalities. A wide range of sulfur-based fragments have been used in the design of low molar mass and dimeric liquid crystals, including terminal alkylthio chains,[49–56] alkylthio spacers,[57–62] thiophene moieties,[33,63] thiocyanate terminal groups,[37,47,64,65] pentafluorosulfanyl terminal groups,[12,66,67] and thioester linking groups.[68–70] Such functionalities have recently been incorporated into molecular structures based on the RM734 archetype[53,71,72] but examples of sulfur-containing ferroelectric nematogens remain minimal.

Here we report thirteen thioester-containing materials, eleven of which exhibit the N_F phase (Table 1). These are RM734-type molecules, with our parent compound **GS36** simply being RM734 with a thioester in place of the ester adjacent to the polar terminus. A selection of structural modifications are made to this backbone, including the position and extent of fluorination, and the nature of lateral and terminal substituents, and the

[a] *Department of Chemistry, University of Aberdeen, Old Aberdeen, AB24 3UE, UK. E-mail: rebecca.walker@abdn.ac.uk*
[b] *Faculty of Chemistry, University of Warsaw, Zwirki i Wigury 101, 02-089 Warsaw, Poland*
† Present Address: School of Pharmacy, Applied Sciences and Public Health, Robert Gordon University, Aberdeen, AB10 7GJ, UK.
‡ Deceased January 2025.

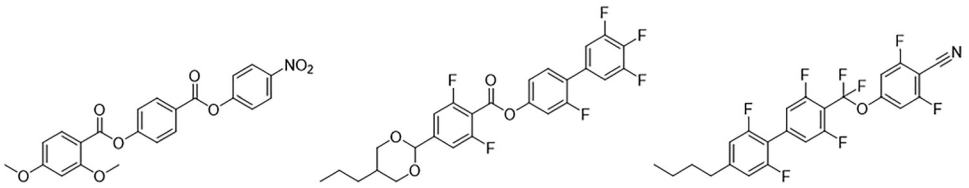

Fig. 1 Molecular structure of (left) RM734, (middle) DIO and (right) UUQU-4N.

Table 1 Molecular structure of the target thioesters, **GS36–48**

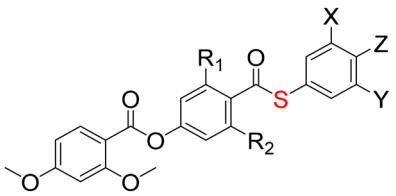

	R_1	R_2	X	Y	Z
GS36	H	H	H	H	NO_2
GS37	H	H	F	H	NO_2
GS38	H	H	F	F	NO_2
GS39	H	F	H	H	NO_2
GS40	F	F	H	H	NO_2
GS41	H	OCH_3	H	H	NO_2
GS42	H	H	H	OCH_3	NO_2
GS43	H	H	F	OCH_3	NO_2
GS44	H	H	H	H	CN
GS45	H	H	H	F	CN
GS46	H	H	F	F	CN
GS47	H	H	H	OCH_3	CN
GS48	H	H	F	OCH_3	CN

Table 2 Molecular structure of the analogous ester-containing materials, **GO1–GO9**

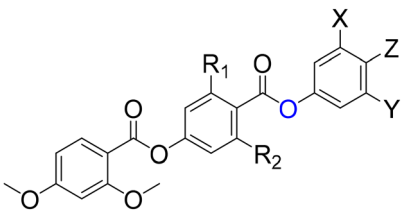

	R_1	R_2	X	Y	Z	Corresponding GS material
GO1	H	H	H	H	NO_2	**GS36**
GO2	H	H	F	H	NO_2	**GS37**
GO3	H	H	F	F	NO_2	**GS38**
GO4	H	F	H	H	NO_2	**GS39**
GO5	F	F	H	H	NO_2	**GS40**
GO6	H	OCH_3	H	H	NO_2	**GS41**
GO7	H	H	H	H	CN	**GS44**
GO8	H	H	F	H	CN	**GS45**
GO9	H	H	F	F	CN	**GS46**

effect of these changes on the phase behaviour is assessed, particularly the stability of the ferroelectric nematic phase. We also compare the thioester-containing compounds to their conventional ester analogues, Table 2, the data for which has either been extracted from our previous literature or re-synthesised for comparison.

Experimental

Synthesis

The synthesis of compounds **GS36–48** consisted of two stages: the preparation of a selection of sulfur-containing intermediates, followed by the synthesis of the final products, see Scheme 1. The preparation of intermediates **4a–4f**, involved three different routes depending on the availability of the starting materials and the different synthetic steps required. In the first step, 4-fluoro-2-methoxybenzonitrile is treated with base to obtain **1a**. In all three routes, the appropriate phenol is reacted with dimethylthiocarbamoyl chloride to produce the *O*-aryl thiocarbamate intermediates **2a–2f**. These are subjected to high temperatures and undergo intramolecular rearrangement, also known as Newman–Kwart rearrangement, to obtain the *S*-aryl thiocarbamate intermediates **3a–3f**, followed by base hydrolysis to yield the required thiophenol-based intermediates, **4a–4f**. The intermediates **4d**, **4e** and **4f** were obtained as mixtures in which the fluorine atom was substituted by a methoxy group, resulting in products A and B. Further details of this are provided in the SI.

The intermediates **5a–d** was prepared by methods reported elsewhere[73,74] and the target molecules **GS36–48** were formed by a Steglich esterification reaction between these and intermediates **4a–f**. A detailed description of the preparation of all the target compounds along with analytical data can be found in the SI.

Characterisation

Mesophase identification from their characteristic optical textures was performed by POM, using an Olympus BH2 polarising light microscope equipped with a Linkam TMS 92 hot stage. Studied samples were sandwiched between two untreated glass coverslips and for characteristic comparison materials were viewed within cells treated for planar alignment, purchased from INSTEC with a thickness between 2.9–3.5 μm and an ITO conducting layer.

Thermal properties of the materials were studied using differential scanning calorimetry performed by a Mettler Toledo DSC1 or DSC3 differential scanning calorimeter equipped with TSO 801RO sample robots and calibrated using indium and zinc standards. Heating and cooling rates were maintained at 10 °C min per minute and all samples were measured under a nitrogen atmosphere. Transition temperatures, which are assigned as the peak maxima, and associated enthalpy changes were extracted from the first heating run unless stated otherwise.

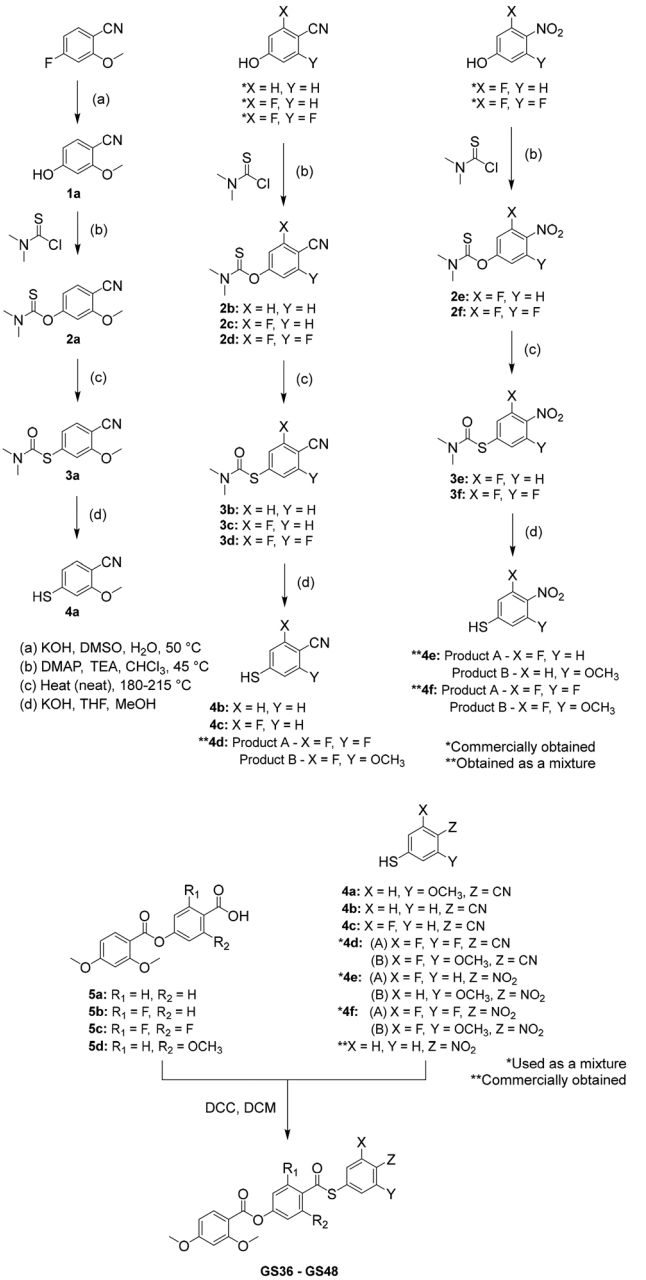

Scheme 1 Synthetic route to target compounds **GS36–48**.

Results and discussion

The thirteen thioester-containing compounds will first be discussed in two sets, split according to the nature of their Z terminus: **GS36–43** contain a terminal nitro group and **GS44–S48** a terminal nitrile group. We will begin by varying the number and substitution pattern of lateral fluorine atoms and methoxy groups within each set of molecules and assessing the resultant mesophase behaviour. Differences in such behaviour upon changing the nature of the terminal group will be considered, and the transitional properties compared to those of corresponding molecules containing an ester rather than thioester linkage.

The effect of lateral substitution in nitro-terminated compounds (GS37–43)

The transitional properties of **GS36–43** are summarised in Table 3. We note that **GS36** has been published elsewhere and transition temperatures obtained here are in excellent agreement with those previously reported.[71] Phase assignments were primarily based on the observation of characteristic textures when the samples were viewed through the polarised optical microscope. Specifically, nematic (N) phases were identified in untreated glass slides by schlieren textures containing two- and four-point brush defects that flashed when subjected to mechanical stress (Fig. 2a), and in cells treated for planar alignment by a uniform texture (Fig. 2b). Additional defect lines appeared when the sample was cooled from the N phase to the

Table 3 Transition temperatures (°C) and associated scaled entropy changes ($\Delta S/R$) for compounds **GS36–48**. The calculated dipole moments (μ, D) are also listed

	μ/D	M.P./°C ($\Delta S/R$)	T_{NFN}/°C *T_{NFI}/°C ($\Delta S/R$)	T_{NI}/°C ($\Delta S/R$)
GS36	12.4	174 (9.0)	107[b]	215 (0.13)
GS37	13.5	186 (16.9)	112[b]	171[a] (0.10)
GS38	13.5	148 (13.1)	*95[a] (0.51)	—
GS39	13.1	184 (14.5)	125[b]	185[a] (0.13)
GS40	12.8	180 (13.4)	132[b]	141[b]
GS41	13.0	165 (13.0)	*108[b]	—
GS42	12.8	151 (11.3)	102[b]	104[b]
GS43	13.0	172 (18.8)	*49[a] (0.93)	—
GS44	12.3	191 (11.6)	—	240 [dec.]
GS45	12.3	212 (14.2)	—	205[a] (0.15)
GS46	14.0	164 (10.7)	143 (0.23)	169[a] (0.11)
GS47	10.5	196 (19.2)	95[b]	123[b]
GS48	10.9	201 (16.7)	*121[a] (1.31)	—

[a] Values extracted from DSC cooling traces. [b] Measured using the polarised optical microscope. [dec.] indicates decomposition prior to clearing.

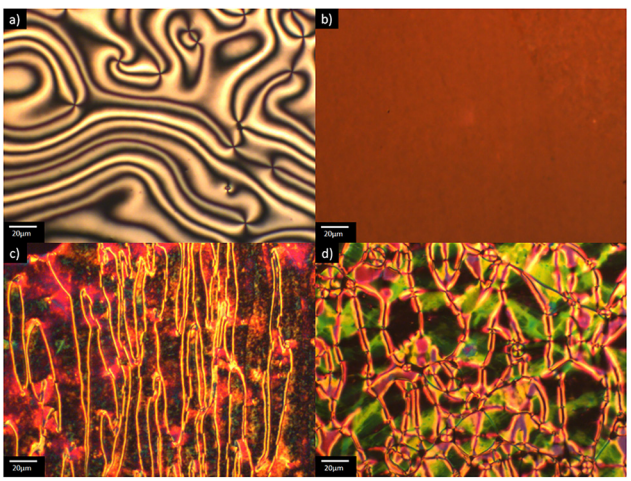

Fig. 2 (a) Schlieren texture of the N phase viewed between untreated glass slides for **GS40** (T = 136 °C); (b) uniform planar texture of the N phase for **GS40** (T = 136 °C); (c) banded texture of the N_F phase for **GS36** (T = 95 °C); (d) banded texture of the N_F phase for **GS38** (T = 87 °C). Textures (b)–(d) were obtained for samples in cells treated for planar alignment.

lower temperature mesophase; the effect was particularly distinct for samples viewed in planar-aligned cells (Fig. 2c) and this so-called 'banded' texture has become characteristic of the ferroelectric nematic phase N_F. Such a texture was also observed following coalescence of spherical droplets upon direct transition from the isotropic to the N_F phase in **GS38**, **41** and **43** (Fig. 2d). These materials are highly monotropic and required significant supercooling to observe the N_F phase, as such many of the temperatures reported were obtained solely from microscope observations. However, where possible scaled entropy changes were obtained from DSC (Table 3). Values of $\Delta S/R$ associated with the direct N_F–I transitions of **GS38** and **GS43** are several times larger than those for N–I transitions in other compounds. This is in accord with data reported for other ferroelectric nematogens having direct N_F–I transitions and is thought to reflect the additional entropic contribution associated with the ordering of the dipoles in the N_F phase.[75–78]

The material containing no additional lateral substituents on the central and right-terminal rings, **GS36**, will be used as a reference against which the effects of fluorine and methoxy substitution will be assessed in molecules **GS37–43** (Fig. 3). The high value of T_{NI} seen for **GS36** may attributed, at least in part, to the thioester linkage which is known to enhance nematic behaviour[68,69,79] and we will return to this point later.

Nematic phase. For all materials reported here, the addition of fluorine substituents led to a decrease in T_{NI}, and this is consistent with previously reported trends.[12,73–77] The effect of adding a single fluorine atom to the terminal ring had a more significant effect on T_{NI} than addition to the central ring. Regardless of which ring it was added to, the addition of a second fluorine substituent had a greater effect than the addition of the first. This may be rationalised as a consequence of the larger steric bulk associated with the F atom, which decreases the overall molecular shape anisotropy and thus lowers T_{NI}. However, this does not fully explain the situation – for example, the reduction in T_{NI} associated with the addition of the second fluorine substituent to the terminal ring in **GS38** seems too large to be accounted for simply in terms of the molecule's aspect ratio, and rather it also acts to further suppress the antiparallel association of molecules. As such associations are known to promote nematic behaviour, we therefore see a significant suppression in T_{NI}.

Introducing an additional lateral methoxy substituent in compounds **GS41–43** greatly destabilised the nematic phase and this presumably reflects the large change in shape, a lowering of the molecular anisotropy and thus a reduction in the ability of the molecule to form antiparallel dimers which drive a conventional nematic arrangement of molecules. Adding the methoxy substituent to the middle ring (**GS41**) led to a loss of the nematic phase entirely, corresponding to a decrease in T_{NI} of at least 100 K compared to the parent compound **GS36**, and of at least 69 K compared to its fluorine substituted analogue **GS37**. Moving the lateral methoxy group from the middle ring to the nitro-substituted terminus to give **GS42** reduced T_{NI} by 111 K compared to **GS36**. **GS43** has both a fluorine and a methoxy substituent on the terminal ring, and, as for the di-fluoro substituted **GS38**, the nematic phase is not observed. This is consistent with previous observations.[74]

Ferroelectric nematic phase. While a large longitudinal molecular dipole appears prerequisite for ferroelectric ordering, there is not a straightforward relationship between the magnitude of the molecular dipole moment and the stability of the N_F phase. The majority of interpretations of structure–property relationships for the N_F phase have been based upon a model proposed by Madhusudana,[80] which describes the molecules as being like rods with regions of alternating positive and negative charge. The electron density present is dictated by the electron-withdrawing or electron-donating nature of the functional groups attached to the aromatic rings. These rod-like molecules can therefore be described by longitudinal surface charge density waves and when the amplitude of these waves is reduced at either end of the molecule formation of the N_F phase is promoted. This can be applied to the structural variations discussed here by considering the effect of the lateral substituents on the distribution of electron density around either the terminal or central ring, depending on their placement.

The addition of a fluorine atom *ortho* to the right-terminal nitro group (**GS37**) enhances T_{NFN} by 5 K. This has been attributed to the fluorine substituent acting to spread electron density more evenly around the terminal ring, reducing the amplitude of the charge density wave and thus stabilising the N_F phase. The effect of adding a fluorine substituent to the middle ring is even more pronounced: the T_{NFN} of **GS39** is increased by 18 K compared to that of the non-fluorinated **GS36**. Comparing the two mono-fluorinated compounds, **GS37** and **GS39**, moving the single additional F atom from the right-terminal to the central ring increases T_{NFN} (by 13 K), despite a

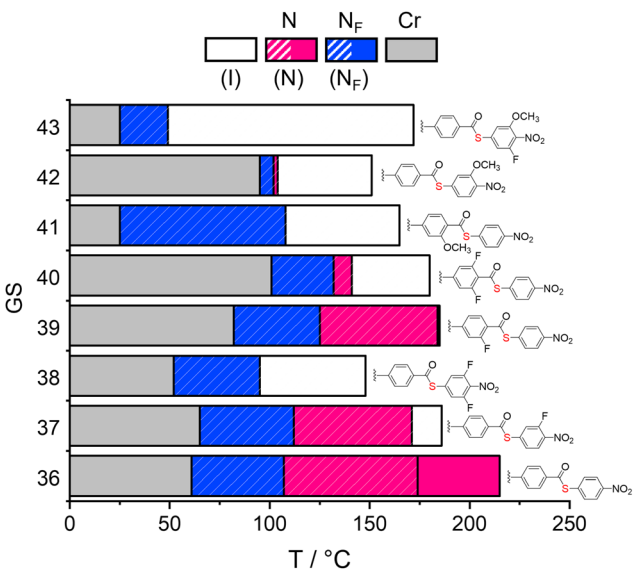

Fig. 3 Comparison of transitional behaviour of **GS36–42**. The T range during which the sample remains isotropic upon supercooling from the clearing point is denoted by (I), Cr indicates the temperature at which the sample recrystallises on supercooling using the polarised optical microscope.

reduction in the overall molecular dipole moment by 0.4 D§ (Table 3) which further highlights that just the dipolar magnitude alone is not enough to predict the behaviour of these compounds as has been previously observed.[15] These observations can be interpreted as an increase in the amplitude of the charge density wave associated with the central ring due to the fluorine substituent, reducing the relative amplitude of the waves at either end of the molecule, and thus stabilising the N_F phase. It is important to note, however, that the accompanying change in molecular shape is not accounted for in this model as it assumes the molecules can be described by similar cylindrical rods. This effect is even greater for **GS40**, with two fluorine substituents on the central ring. **GS40** has the highest T_{NFN} of this trio, elevated by 25 K and 7 K from **GS36** and **GS39**, respectively. These differences may be attributed to a combination of (i) a favourable change in molecular shape and (ii) a further increase in the amplitude of the charge density wave on the fluorine-substituted central ring relative to that of the terminus. However, this framework does not fully explain the behaviour of **GS38**, with two fluorine substituents on the right-terminal ring. For this material, the addition of the second fluorine atom has a detrimental effect on the stability of the N_F phase, lowering T_{NFI} by 17 K and 12 K compared to **GS37** and **GS36**, respectively. In terms of the Madhusudana model, the reason for this decrease is not immediately apparent.[80] The addition of a second F atom would contribute to a further spread of the electronic charge more evenly around the right-terminus, reducing the amplitude of the charge density wave, and thus an increase in T_{NFI} might have been expected. Presumably, this effect is offset by an unfavourable change in the molecular shape.

The application of this framework is further complicated by the more pronounced changes in molecular shape produced by methoxy substituents. According to the Madhusudana model, the electron donating methoxy group acts to increase electron density in the ring to which it is attached.[80] In such terms, the inclusion of a methoxy substituent on the middle ring (**GS41**) would be expected to promote the N_F phase. However, T_{NFI} of **GS41** is essentially the same as T_{NFN} of **GS36**. In addition, T_{NFI} for **GS41** is lower by 17 K than T_{NFN} of its fluorine-substituted analogue **GS39**. This appears to highlight the importance of shape effects from the larger methoxy group. **GS42**, in which the methoxy substituent is added *ortho* to the terminal nitro group, has a substantially lower T_{NI} – by over 100 K – than the unsubstituted **GS36**, attributed to a decrease in molecular anisotropy, as discussed in the previous section. However, T_{NFN} for **GS42** is significantly less affected, with a decrease of only 5 K. This suggests that, in this case, the detrimental effect of molecular shape is at least somewhat counteracted by favourable electronic factors which act to stabilise the ferroelectric nematic phase. Namely, in the same manner as *ortho* fluorine substituents in **GS37** and **GS38**, the methoxy group acts to decrease the amplitude of the charge density wave at the end of the molecule by spreading the charge around the terminal substituents. The net effect is therefore a much smaller decrease in T_{NFN} than in T_{NI}, which is less sensitive to electronic effects.

A fluorine atom is added *ortho* to the terminal nitro group in **GS42** to give the 3,4,5-terminated **GS43** and this results in a decrease in T_{NF-} of 53 K. This is consistent with the trend seen with the di-fluoro substituted **GS38**, for which the second substituent *ortho* to the terminal nitro group destabilises the N_F phase. A final comparison between **GS38** (3,4,5-terminated where positions 3 and 5 are F) and **GS43** (3,4,5-terminated where position 3 is OMe and 5 is F) sees a reduction of T_{NFI} by 46 K on substituting F with OMe. This is an even more pronounced decrease than that produced by the analogous substitution between **GS37** and **GS42** (10 K). These observations suggest that, in nitro-terminated molecules, this di-substitution is not conducive to the parallel association of the molecules, *i.e.* a ferroelectric arrangement, and this is exacerbated by the associated change in shape.

The effect of lateral substitution in nitrile-terminated compounds (GS44–48)

We now turn our attention to five nitrile-terminated compounds for which the additional substituents on this terminal ring are varied while the rest of the molecule remains unchanged. The phase behaviour for these is also summarised in Table 2 and assignments again made based on characteristic optical textures. **GS44** is the nitrile-terminated analogue of **GS36**, and we will use this as a reference against which the effects of structural modifications are assessed (Fig. 4).

Nematic phase. **GS44** melts directly into the conventional nematic phase and begins to decompose above 240 °C. This exceptionally high T_{NI} is presumably due to the combined effect of the terminal nitrile group and thioester linkage, the inclusion of both is known to increase the stability of the nematic phase.[12,79] The addition of lateral fluoro or methoxy substituents destabilised the nematic phase relative to **GS44**, consistent

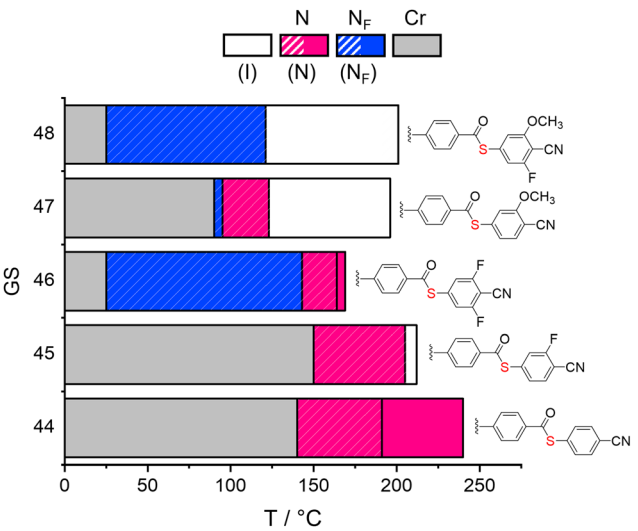

Fig. 4 Comparison of transitional behaviour of **GS44–48**. The *T* range during which the sample remains isotropic upon supercooling from the clearing point is denoted by (I), Cr indicates the temperature at which the sample recrystallises on supercooling using the polarised optical microscope.

§ The molecular dipole moments were calculated using Orca 6.0.1,[82–87] performed using the r^{2}SCAN-D4 functional with the def2-TZVP basis set.

with the effects previously discussed for the nitro-terminated materials.

Ferroelectric nematic phase. **GS44** and **GS45** do not exhibit the N_F phase, and their N phases may be cooled to 140 °C and 150 °C, respectively, prior to crystallisation. The inclusion of a second fluorine substituent *ortho* to the nitrile group (**GS46**) led to a significant decrease in the melting temperature, and to the onset of crystallisation on cooling which revealed a monotropic N_F–N transition. The presence of two fluorine atoms *ortho* to the nitrile group appear to inhibit the antiparallel associations of these nitrile-terminated molecules, which promotes the formation of the N_F phase. Such a destabilisation of antiparallel correlations was similarly described for conventional nematogens.[81]

Somewhat surprisingly, **GS47**, with a methoxy substituent *ortho* to the nitrile group, also exhibits a monotropic N_F–N transition. The addition of a fluorine atom *ortho* to the terminal nitrile group in **GS47** to give **GS48** resulted in a direct N_F–I transition. The value of T_{NFI} for **GS48** is 26 K higher than T_{NFN} for **GS47**. In contrast, comparing **GS48** with **GS46**, the change from a fluorine to a methoxy substituent reduced T_{NFN} by at least 22 K.

It seems that while a single substituent *ortho* to the nitrile terminus is detrimental to both nematic phases, the N_F phase is re-stabilised by the introduction of a second substituent *ortho* to CN, presumably as a result of the double substitution effectively disrupting antiparallel packing of molecules and promoting a ferroelectric arrangement.

Comparing terminal nitro and nitrile groups. Fig. 5 compares the values of T_{NI}, and $T_{NFN/NFI}$ between corresponding pairs of molecules where the only structural difference is the nature of the polar terminal group (*e.g.* **GS36** with **GS44**). It is clear that the nitrile terminal group is more efficient in promoting the conventional nematic phase; and a similar trend in the values of T_{NI} was observed previously between corresponding nitro- and nitrile-containing compounds.[12] This can be attributed to the fact that nitrile-substituted compounds typically exhibit enhanced shape anisotropy and a greater ability to form antiparallel dimers.

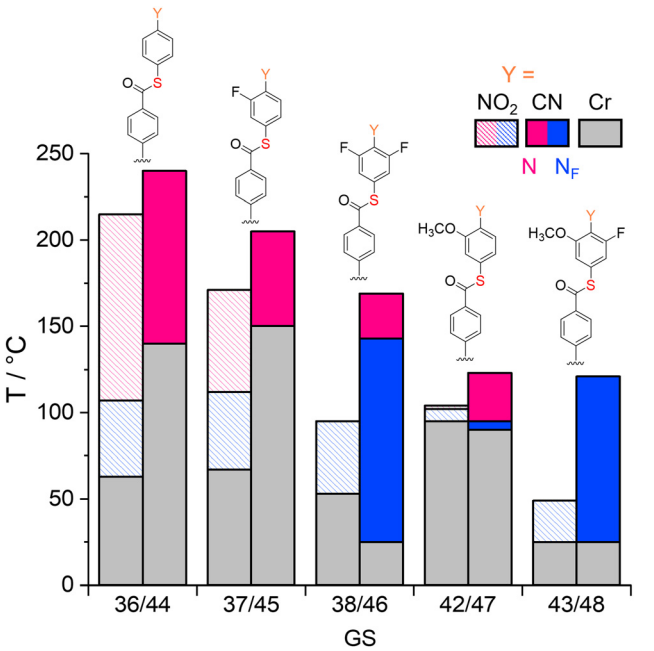

Fig. 5 Transitional behaviour of **GS36–48**, comparing cyano and nitro terminal groups. Cr indicates the temperature at which the sample recrystallises on supercooling using the polarised optical microscope.

The trend in the values of T_{NFN}/T_{NFI} between these two groups of compounds is more variable. Of the three pairs for which a comparison is possible, the nitrile-substituted compound shows significantly higher transition temperatures in two cases (**GS38**/**46** and **GS43**/**48**), but this trend is reversed in the third. It is apparent that there is no simple relationship with the dipole moments of these pairs. It appears that two substituents at positions *ortho* to a nitrile group are required to significantly inhibit the antiparallel associations which promote N phase behaviour, and when this is the case, the resulting shape of these molecules is more conducive to the formation of the N_F phase than that of their nitro-terminated analogues. For nitrile-terminated materials with only one *ortho*-substituent, (*e.g.* **GS47**) the formation of antiparallel dimers is still possible, which decreases the stability of the N_F phase relative to the N phase, and hence the inversion of T_{NFN} for **GS47** and **GS42** is seen. The early onset of crystallisation observed for **GS45** prevented this comparison from being extended to the equivalent single fluorinated derivative.

Thioester *vs.* ester

Nine of the new thioester-containing materials **GS36–41** and **44–46** can be compared to the corresponding compounds containing an ester link. The structures of the ester-containing molecules are given in Table 2, and their transitional properties in Table S1. These materials have previously been published by us and others, and the transitional properties obtained here are generally in excellent agreement with literature. An exception is compound **GO9**, which contains F atoms in the two positions *ortho* to a nitrile terminal group. **GO9** was found to exhibit a direct N_F–I transition at 150 °C, while previously it was reported to be solely nematogenic.

For all pairs, T_{NI} is higher for the thioester-containing compounds, as can be seen in Fig. 6. This is consistent with previously observed trends for liquid crystals comparing thioester and ester linkages. The thioester linkage makes the overall molecular shape longer and more anisotropic than the corresponding ester[71] and the larger, more electron-rich, and highly polarisable sulfur atom acts to enhance intermolecular interactions.

Conversely, in all but two cases, T_{NFN}/T_{NFI} is reduced by the presence of the sulfur-based group. This can be rationalised by electronic differences between oxygen and sulfur atoms. Specifically, delocalisation of electrons between the heteroatom (either O or S) and the carbonyl group is less effective for sulfur because the energy gap between sulfur's 3p orbital and the carbonyl π-system is larger compared to that of the equivalent oxygen orbital (2p). However, sulfur's electrons can more effectively interact with the π-system of the terminal ring such that, in contrast to the ester-linked materials, the terminal ring is more electron-rich. Consequently, the amplitude of the charge density wave at this terminus is increased and the N_F phase is destabilised. We will return to the exceptional cases below.

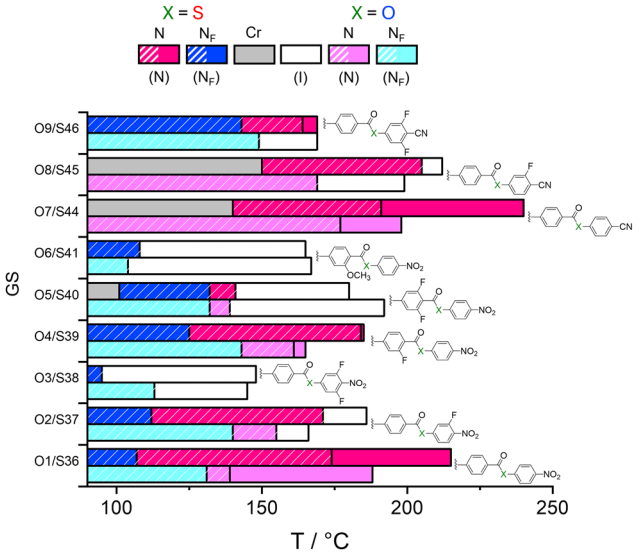

Fig. 6 Comparison of the transition temperatures for the ester (**O1–O9**) and thioester-linked (**S36–46**) compounds. The *T* range during which the sample remains isotropic upon supercooling from the clearing point is denoted by (I), Cr indicates the temperature at which the sample recrystallises on supercooling using the polarised optical microscope.

Increasing the number of F substituents on the polar terminus has a similar effect on both ester- and thioester-containing materials (**O1–3** and **S36–38**) such that T_{NI} is highest for the non-fluorinated materials (**O1**/**S36**) and the singly fluorinated analogues (**O2**/**S37**) show the highest temperature N_F phase, the reasons for which were discussed earlier. The addition of lateral substituents on the central ring (**O4–O6**, **S39–41**) appears to have a greater effect on the N_F phase for the thioesters. **GS39**, with one F substituent, has a lower T_{NFN} compared to **GO4**. However, the effect of the second fluorine is dependent on the nature of the linkage: ester-linked material **GO5** has a lower T_{NFN} than **GO4**, while T_{NFN} of the thioester-linked **GS40** is enhanced compared to **GS39**; **GO5** and **GS39** therefore coincidentally have identical values of T_{NFN}. For both the thioester and ester linked compounds, the electronic effects of adding a single fluorine to the middle ring enhances T_{NFN}, as discussed earlier, and appears to overcome any detrimental changes to molecular shape. However, while the addition of a second fluorine also has this favourable electronic effect, the accompanying changes to molecular shape appear to vary depending on the nature of the linking group. Specifically, the unsubstituted thioester **GS36** has a more anisotropic shape than the corresponding oxygen material RM734, which has been interpreted as being unfavourable due to the potential for antiparallel interactions which according to the predictions of Madhusudana inhibits the formation of the N_F phase.[80] This is indeed reflected in their respective N_F–N transition temperatures, and this is also true for the singly substituted (**GS39** and **GO4**). For the more favourably shaped oxygen-based materials, the addition of a second fluorine substituent appears to have a detrimental effect on molecular shape, to a large enough extent that it offsets the favourable electronic changes. In contrast, the detrimental effect on the molecular shape endowed by the inclusion of the second fluorine atom appears to be less significant in the thioester compounds, due to their less favourable starting shape, such that the cumulative steric and electronic effects are dominated by the latter and enhance the stability of the N_F phase. This is even more pronounced for compounds with a single lateral methoxy group in the middle ring, which acts to drastically reduce T_{NI} in both types of material: **GO6** *vs.* **GO1**, **GS41** *vs.* **GS36**. In the ester compounds T_{NF-} is also significantly reduced, while its thioester counterpart maintains a nearly identical T_{NF-} to the non-substituted material, such that now T_{NFI} **GS41** > T_{NFI} **GO6**.

Molecules with a nitrile terminus (**GO7–9** *vs.* **GS44–46**) share the expected increase in T_{NI} on replacing an ester with a thioester linkage. Only the pair with two F atoms *ortho* to the polar terminus (**GO9**, **GS46**) exhibit an N_F phase, for reasons discussed earlier, but the sulfur-containing material is the only one to show both N and N_F phases. This is presumably a consequence of the stability endowed to the N phase by the thioester moiety, in conjunction with that provided by the nitrile group. The molecular dipole moment of **GS46** is only 0.1 D higher than its ester-containing counterpart, and the latter has the higher T_{NFN} by 6 K. The C–S–C bond in the thioester enhances the overall linearity of the molecules compared to the C–O–C bond of an ester, and consequently causes the magnitude of the overall molecular dipole moment to be higher as well as the value of T_{NI}.[71] The value of T_{NFN}, however, falls and this is likely due to the mesogens favouring antiparallel correlations preferable for the conventional nematic phase rather than the parallel correlations favoured by the N_F phase thanks to the shape and electronic profile of the molecule.

Conclusions

We have reported thirteen sulfur-based liquid crystals based on the molecular backbone of RM734 and containing thioester linkages, ten of which are new ferroelectric nematogens. Phase transition temperatures are compared for systematic changes to molecular structure including the position and extent of fluorination, and the nature of lateral and terminal substituents. The new materials are compared with their ester-linked counterparts, including one for which phase behaviour has been reassigned from solely nematic to solely ferroelectric nematic. In line with expected behaviour of the nematic phase, replacement of an ester with a thioester raised T_{NI}, but N_F phase stability upon making this change proved more variable. These findings remain in line with the general view that the formation of the N_F phase is not solely governed by the magnitude of the molecular dipole moment, but able to be tuned by the interplay of steric and electronic effects endowed by different molecular fragments.

Author contributions

GS, SB and EC synthesised the reported compounds. GS, SB, EC, RW performed thermal and optical analyses. Interpretation of results was performed by GS, CTI, EC, GJS and RW. CTI and

JMDS proposed the project and acquired funding. RW, GJS and EC wrote and edited the original manuscript; all authors provided input to the final manuscript.

Conflicts of interest

There are no conflicts to declare.

Data availability

The data supporting this article have been included as part of the supplementary information (SI). Supplementary information is available. See DOI: https://doi.org/10.1039/d5sm01206f.

Acknowledgements

Thank you to Marijus Juodka for helpful discussions regarding Orca calculations. The authors would like to acknowledge the immense contributions to this project, as well as past, ongoing present, and future work by Professor CT Imrie, who passed away suddenly in January 2025. CTI and JMDS acknowledge the financial support of the Engineering and Physical Sciences Research Council [EP/V048775/1].

References

1 X. Chen, E. Korblova, D. Dong, X. Wei, R. Shao, L. Radzihovsky, M. A. Glaser, J. E. MacLennan, D. Bedrov, D. M. Walba and N. A. Clark, *Proc. Natl. Acad. Sci. U. S. A.*, 2020, **117**, 14021–14031.
2 F. Caimi, G. Nava, R. Barboza, N. A. Clark, E. Korblova, D. M. Walba, T. Bellini and L. Lucchetti, *Soft Matter*, 2021, **17**, 8130–8139.
3 P. Rudquist, *Sci. Rep.*, 2021, **11**, 24411.
4 C. L. Folcia, J. Ortega, R. Vidal, T. Sierra and J. Etxebarria, *Liq. Cryst.*, 2022, **49**, 899–906.
5 H. Nishikawa, K. Sano, S. Kurihara, G. Watanabe, A. Nihonyanagi, B. Dhara and F. Araoka, *Commun. Mater.*, 2022, **3**, 89.
6 C. Parton-Barr, H. F. Gleeson and R. J. Mandle, *Soft Matter*, 2024, **20**, 672–680.
7 A. Erkoreka and J. Martinez-Perdiguero, *Phys. Rev. E*, 2024, **110**, L022701.
8 J. Szydlowska, P. Majewski, M. Čepič, N. Vaupotič, P. Rybak, C. T. Imrie, R. Walker, E. Cruickshank, J. M. D. Storey, P. Damian and E. Gorecka, *Phys. Rev. Lett.*, 2023, **130**, 216802.
9 M. T. Máthé, B. Farkas, L. Péter, Á. Buka, A. Jákli and P. Salamon, *Sci. Rep.*, 2023, **13**, 6981.
10 N. Sebastián, R. J. Mandle, A. Petelin, A. Eremin and A. Mertelj, *Liq. Cryst.*, 2021, **48**, 2055–2071.
11 R. J. Mandle, S. J. Cowling and J. W. Goodby, *Phys. Chem. Chem. Phys.*, 2017, **19**, 11429–11435.
12 R. J. Mandle, S. J. Cowling and J. W. Goodby, *Chem. – Eur. J.*, 2017, **23**, 14554–14562.
13 H. Nishikawa, K. Shiroshita, H. Higuchi, Y. Okumura, Y. Haseba, S. I. Yamamoto, K. Sago and H. Kikuchi, *Adv. Mater.*, 2017, **29**, 1702354.
14 A. Manabe, M. Bremer and M. Kraska, *Liq. Cryst.*, 2021, **48**, 1079–1086.
15 E. Cruickshank, *ChemPlusChem*, 2024, e202300726.
16 J. Li, Z. Wang, M. Deng, Y. Zhu, X. Zhang, R. Xia, Y. Song, Y. Hisai, S. Aya and M. Huang, *Giant*, 2022, **11**, 100109.
17 R. J. Mandle, *Soft Matter*, 2022, **18**, 5014–5020.
18 Y. Song, S. Aya and M. Huang, *Giant*, 2024, **19**, 100318.
19 D. Pociecha, R. Walker, E. Cruickshank, J. Szydlowska, P. Rybak, A. Makal, J. Matraszek, J. M. Wolska, J. M. D. Storey, C. T. Imrie and E. Gorecka, *J. Mol. Liq.*, 2021, **361**, 119532.
20 X. Zhao, J. Zhou, J. Li, J. Kougo, Z. Wan, M. Huang and S. Aya, *Proc. Natl. Acad. Sci. U. S. A.*, 2021, **118**, e2111101118.
21 C. Feng, R. Saha, E. Korblova, D. Walba, S. N. Sprunt, A. Jákli, C. Feng, S. N. Sprunt, A. Jákli, R. Saha, E. Korblova and D. Walba, *Adv. Opt. Mater.*, 2021, **9**, 2101230.
22 H. Nishikawa and F. Araoka, *Adv. Mater.*, 2021, **33**, 2101305.
23 J. Hobbs, C. J. Gibb, D. Pociecha, J. Szydłowska, E. Górecka and R. J. Mandle, *Angew. Chem., Int. Ed.*, 2025, **64**, e202416545.
24 Y. Song, M. Deng, Z. Wang, J. Li, H. Lei, Z. Wan, R. Xia, S. Aya and M. Huang, *J. Phys. Chem. Lett.*, 2022, **13**, 9983–9990.
25 X. Chen, V. Martinez, P. Nacke, E. Korblova, A. Manabe, M. Klasen-Memmer, G. Freychet, M. Zhernenkov, M. A. Glaser, L. Radzihovsky, J. E. Maclennan, D. M. Walba, M. Bremer, F. Giesselmann and N. A. Clark, *Proc. Natl. Acad. Sci. U. S. A.*, 2022, **119**, e2210062119.
26 H. Nishikawa, M. Kuwayama, A. Nihonyanagi, B. Dhara and F. Araoka, *J. Mater. Chem. C*, 2023, **11**, 12525–12542.
27 H. Kikuchi, H. Matsukizono, K. Iwamatsu, S. Endo, S. Anan and Y. Okumura, *Adv. Sci.*, 2022, **9**, 2202048.
28 H. Kikuchi, H. Nishikawa, H. Matsukizono, S. Iino, T. Sugiyama, T. Ishioka and Y. Okumura, *Adv. Sci.*, 2024, **11**, 2409827.
29 J. Hobbs, C. J. Gibb and R. J. Mandle, *Small Sci.*, 2024, **4**, 2400189.
30 G. J. Strachan, S. J. Ramsay, M. Juodka, D. Pociecha, J. Szydlowska, J. Storey, N. Vaupotič, R. Walker, E. Gorecka, G. J. Strachan, D. Pociecha, J. Szydlowska, E. Gorecka, S. J. Ramsay, M. Juodka, J. M. Storey, R. Walker and N. Vaupotič, *Angew. Chem.*, 2025, e202516302.
31 H. Nishikawa, Y. Okumura, D. Kwaria, A. Nihonyanagi and F. Araoka, *Adv. Mater.*, 2025, 2501946.
32 Y. Song, X. Huang, X. Zhang, M. Deng, S. Aya, M. Huang, Y. Song, X. Huang, X. Zhang, M. Deng, S. Aya and M. Huang, *Adv. Sci.*, 2025, 2414317.
33 E. Cruickshank, P. Rybak, M. M. Majewska, S. Ramsay, C. Wang, C. Zhu, R. Walker, J. M. D. Storey, C. T. Imrie, E. Gorecka and D. Pociecha, *ACS Omega*, 2023, **8**, 36562–36568.
34 P. Nacke, A. Manabe, M. Klasen-Memmer, X. Chen, V. Martinez, G. Freychet, M. Zhernenkov, J. E. Maclennan, N. A. Clark, M. Bremer and F. Giesselmann, *Sci. Rep.*, 2024, **14**, 1–13.
35 X. Chen, V. Martinez, E. Korblova, G. Freychet, M. Zhernenkov, M. A. Glaser, C. Wang, C. Zhu, L. Radzihovsky, J. E. Maclennan,

D. M. Walba and N. A. Clark, *Proc. Natl. Acad. Sci. U. S. A.*, 2022, **120**, e2217150120.
36 M. Mrukiewicz, M. Czerwiński, N. Podoliak, D. Repček, P. Perkowski, R. J. Mandle and D. Węgłowska, *J. Mater. Chem. C*, 2024, **12**, 7214–7224.
37 R. J. Mandle, *Liq. Cryst.*, 2023, **50**, 534–542.
38 C. J. Gibb, J. Hobbs, D. I. Nikolova, T. Raistrick, S. R. Berrow, A. Mertelj, N. Osterman, N. Sebastián, H. F. Gleeson and R. J. Mandle, *Nat. Commun.*, 2024, **15**, 5845.
39 D. Pociecha, J. Szydlowska, N. Vaupotič, K. Kwiatkowska, M. Juodka, J. Spiess, J. M. D. Storey, C. T. Imrie, R. Walker and E. Gorecka, *Adv. Sci.*, 2025, e08405.
40 J. Karcz, J. Herman, N. Rychłowicz, P. Kula, E. Górecka, J. Szydlowska, P. W. Majewski and D. Pociecha, *Science*, 2024, **384**, 1096–1099.
41 H. Nishikawa, D. Okada, D. Kwaria, A. Nihonyanagi, M. Kuwayama, M. Hoshino and F. Araoka, *Adv. Sci.*, 2024, **11**, 2405718.
42 E. Gorecka, M. Majewska, L. Fekete, J. Karcz, J. Żukowska, J. Herman, P. Kula and D. Pociecha, *Mater. Horiz.*, 2025, **12**, 5352–5356.
43 J. Hobbs, C. J. Gibb and R. J. Mandle, *Nat. Commun.*, 2025, **16**, 7510.
44 Z. Raszewski, W. Piecek, L. Jaroszewicz, E. Nowinowski-Kruszelnicki, P. Perkowski, L. Soms, R. Dabrowski, J. Kedzierski, M. Olifierczuk, M. Mrukiewicz, E. Miszczyk, P. Morawiak, R. Mazur and K. Kowiorski, *Adv. Mater. Res.*, 2014, **909**, 12–18.
45 N. Bennis, T. Jankowski, O. Strzezysz, A. Pakua, D. C. Zografopoulos, P. Perkowski, J. M. Sánchez-Pena, J. M. López-Higuera and J. F. Algorri, *Sci. Rep.*, 2022, **12**, 012107.
46 M. Reuter, N. Vieweg, B. M. Fischer, M. Mikulicz, M. Koch, K. Garbat and R. Dąbrowski, *APL Mater.*, 2013, **1**, 012107.
47 M. Hird, A. J. Seed, K. J. Toyne, J. W. Goodby, G. W. Gray and D. G. McDonnell, *J. Mater. Chem.*, 1993, **3**, 851–859.
48 Y. Arakawa, Y. Sasaki, N. Haraguchi, S. Itsuno and H. Tsuji, *Liq. Cryst.*, 2018, **45**, 821–830.
49 E. Cruickshank, G. J. Strachan, J. M. D. Storey and C. T. Imrie, *J. Mol. Liq.*, 2021, **346**, 117094.
50 Y. Arakawa, S. Inui and H. Tsuji, *Tetrahedron*, 2022, **122**, 132958.
51 Y. Arakawa, Y. Ishida, T. Shiba, K. Igawa, S. Sasaki and H. Tsuji, *CrystEngComm*, 2022, **24**, 1877–1890.
52 E. Cruickshank, R. Walker, G. J. Strachan, C. H. F. Goode, M. M. Majewska, D. Pociecha, E. Gorecka, J. M. D. Storey and C. T. Imrie, *J. Mol. Liq.*, 2023, **391**, 123226.
53 G. Stepanafas, E. Cruickshank, S. Brown, M. M. Majewska, D. Pociecha, E. Gorecka, J. M. D. Storey and C. T. Imrie, *Mater. Adv.*, 2024, **5**, 525–538.
54 M. Alaasar, C. Anders, R. Pashameah and A. F. Darweesh, *Liq. Cryst.*, 2023, **50**, 2397–2412.
55 R. Saha, C. Feng, C. Welch, G. H. Mehl, J. Feng, C. Zhu, J. Gleeson, S. Sprunt and A. Jákli, *Phys. Chem. Chem. Phys.*, 2021, **23**, 4055–4063.
56 E. Cruickshank, G. J. Strachan, M. M. Majewska, D. Pociecha, E. Gorecka, J. M. D. Storey and C. T. Imrie, *J. Mater. Chem. C*, 2025, **13**, 20156–20168.
57 E. Cruickshank, M. Salamończyk, D. Pociecha, G. J. Strachan, J. M. D. Storey, C. Wang, J. Feng, C. Zhu, E. Gorecka and C. T. Imrie, *Liq. Cryst.*, 2019, **46**, 1595–1609.
58 Y. Arakawa, K. Komatsu and H. Tsuji, *New J. Chem.*, 2019, **43**, 6786–6793.
59 Y. Arakawa, Y. Arai, K. Horita, K. Komatsu and H. Tsuji, *Crystals*, 2022, **12**, 1734.
60 Y. Arakawa, Y. Ishida, K. Komatsu, Y. Arai and H. Tsuji, *Tetrahedron*, 2021, **95**, 132351.
61 Y. Arakawa and Y. Arai, *Materials*, 2024, **17**, 3278.
62 E. Cruickshank, G. J. Strachan, A. Pearson, D. Pociecha, E. Gorecka, J. M. D. D. Storey and C. T. Imrie, *Phys. Chem. Chem. Phys.*, 2025, **27**, 6111–6121.
63 A. Seed, *Chem. Soc. Rev.*, 2007, **36**, 2046–2069.
64 G. J. Cross, A. J. Seed, K. J. Toyne, J. W. Goodby, M. Hird and M. C. Artal, *J. Mater. Chem.*, 2000, **10**, 1555–1563.
65 R. J. Mandle, E. J. Davis, C. C. A. Voll, C. T. Archbold, J. W. Goodby and S. J. Cowling, *Liq. Cryst.*, 2015, **42**, 688–703.
66 M. V. Ponomarenko, N. Kalinovich, Y. A. Serguchev, M. Bremer and G. V. Röschenthaler, *J. Fluorine Chem.*, 2012, **135**, 68–74.
67 J. A. Smith, R. A. DiStasio, N. A. Hannah, R. W. Winter, T. J. R. Weakley, G. L. Gard and S. B. Rananavare, *J. Phys. Chem. B*, 2004, **108**, 19940–19948.
68 A. J. Seed, K. J. Toyne, J. W. Goodby and D. G. McDonnell, *J. Mater. Chem.*, 1995, **5**, 1–11.
69 Z. Fang and C. Wu, *Liq. Cryst.*, 2020, **47**, 1086–1099.
70 A. U. Petersen, M. Jevric, R. J. Mandle, M. D. Kilde, F. P. Jørgensen, J. W. Goodby and M. B. Nielsen, *Aust. J. Chem.*, 2018, **71**, 422–434.
71 Y. Arakawa, Q. Ning, S. Karthick and S. Aya, *J. Mater. Chem. C*, 2024, **12**, 16206–16217.
72 P. Guragain, A. Ghimire, M. Badu, N. P. Dhakal, P. Nepal, J. T. Gleeson, S. Sprunt, R. J. Twieg and A. Jákli, *Mater. Horiz.*, 2025, **12**, 8153–8164.
73 S. Brown, E. Cruickshank, J. M. D. Storey, C. T. Imrie, D. Pociecha, M. Majewska, A. Makal and E. Gorecka, *ChemPhysChem*, 2021, **22**, 2506–2510.
74 E. Cruickshank, N. Tufaha, R. Walker, S. Brown, E. Gorecka, D. Pociecha, J. M. D. Storey and C. T. Imrie, *Liq. Cryst.*, 2024, **51**, 401–415.
75 N. Tufaha, E. Cruickshank, D. Pociecha, E. Gorecka, J. M. D. Storey and C. T. Imrie, *Chem. – Eur. J.*, 2023, **29**, e202300073.
76 E. Cruickshank, R. Walker, J. M. D. Storey and C. T. Imrie, *RSC Adv.*, 2022, **12**, 29482–29490.
77 E. Cruickshank, R. Walker, M. M. Majewska, E. Gorecka, D. Pociecha, J. M. D. Storey and C. T. Imrie, *ACS Omega*, 2025, **10**, 23609–23619.
78 E. Cruickshank, R. Walker, G. J. Strachan, E. Górecka, D. Pociecha, J. M. D. Storey and C. T. Imrie, *J. Mater. Chem. C*, 2025, **13**, 3902–3916.
79 U. Jarek-Mikulska and Z. Galewski, *Liq. Cryst.*, 2009, **36**, 187–195.
80 N. V. Madhusudana, *Phys. Rev. E*, 2021, **104**, 014704.
81 J. E. Fearon, G. W. Gray, A. D. Ifill and K. J. Toyne, *Mol. Cryst. Liq. Cryst.*, 1985, **124**, 89–103.

82 F. Neese, *Wiley Interdiscip. Rev.:Comput. Mol. Sci.*, 2012, **2**, 73–78.
83 F. Neese, F. Wennmohs, U. Becker and C. Riplinger, *J. Chem. Phys.*, 2020, **152**, Art. No. L224108.
84 F. Neese, *Wiley Interdiscip. Rev.:Comput. Mol. Sci.*, 2022, **12**, e1606.
85 F. Neese, *Chem. Phys. Lett.*, 2000, **325**, 93–98.
86 F. Neese, *J. Comput. Chem.*, 2022, 1–16.
87 F. Neese, *J. Comput. Chem.*, 2003, **24**, 1740–1747.